RSC Advances

ROYAL SOCIETY OF CHEMISTRY

www.rsc.org/advances

Quaternized Mesoporous Silica/polysulfone Composite Membrane for an efficient alkaline fuel cell application

Vijayakumar Elumalai and Dharmalingam Sangeetha *

Department of Mechanical Engineering, Anna University, Chennai - 600 025, India

Email: sangeetha@annauniv.edu

Phone: +91- 44- 2235 7763, Fax: +91- 44- 2235 7744

Graphical Abstract

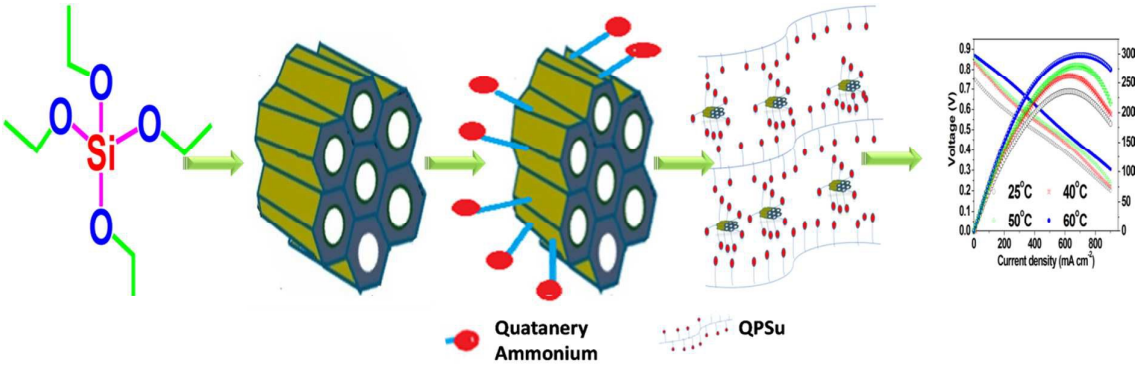

Abstract:

Mesoporous silica (SBA-15) was synthesized and quaterinzed via chloromethylation followed by amination. Quaterinzed SBA-15 (QSBA) was characterized by FTIR, solid state C^{13} NMR, BET, XRD and TEM. QSBA was then incorporated into quaternary polysulfone (QPSu) in different weight percentage (1-4%) to form high ion exchange capacity composite membranes. The composite membranes were analysed by SEM and XRD. The water uptake, ion exchange capacity and hydroxyl conductivity of the composite membrane were studied for the suitability of the membrane in alkaline fuel cell. Membrane electrode assembly was constructed using carbon supported platinum (Vulcan XC-72) anode, cathode catalysts and QPSU/3%QSBA-15 composite membrane and tested in an AFC. A maximum power density of 298 mW/cm^2 was achieved at 60ºC. Experimental results showed that the QPSU/QSBA-15 composite membrane exhibited promising electrochemical performance in an AFC.

Keywords: SBA-15, Quarternized Polysulfone, Anion functionalized filler, Conductivity AEMFC,

1. Introduction:

At present, in the search of fuel cell as alternate energy producing devices, the development of Anion Exchange Membrane Fuel Cell (AEMFC) has been receiving increased attention over other fuel cell types due to its rapid reaction kinetics in the alkaline medium, improved water management and use of non-noble electrode catalysts[1–5]. The working principle of AEMFC is similar to that of the alkaline fuel cell (AFC) working with potassium hydroxide as electrolyte [6]. In AEMFCs, the Anion Exchange Membrane (AEM) is the key component, in which the polymers carry fixed cation head groups surrounded with mobile negatively charged hydroxyl group[7]. Although it is promising, for the improved performance of alkaline membranes, it still needs detailed study before this technology is ready for commercialization.

AEMFCs has considerable advantages over PEMFC, however their low ionic conductivity is a matter of concern because it would potentially lead to lower performance[8]. For the development of a superior AEM, the important parameters to be considered include high ionic conductivity, water retention, and physico-chemical stability[9] . From the works of various researchers, it was noted that, inevitably, achieving one desirable property of AEMs was usually at the cost of other parameters. For example, making the membranes highly conductive requires high degree of quaternization which has a drastic negative effect on the membrane's mechanical, thermal and chemical stabilities [10]. Synthesis of AEM having high ionic conductivity along with suitable mechanical stability for long term fuel cell power generation has continued to be the focus of research worldwide[11–14].

Composite membranes are potential candidates for the developments in AEM to overcome the challenges discussed above. Few inorganic fillers such as SiO_2[15], ZrO_2 [16] TiO_2 [14] have been incorporated in different AEM membranes and their performances were studied. The results reported that these composite membranes displayed overall better properties than the bare membranes. The key role of the inorganic fillers in the composite membranes is to increase the water retention that improves conductivity, while simultaneously maintaining good mechanical and thermal stability[17]. These nano sized inorganic materials have advantages such as high surface area and excellent chemical stability. In addition, when ionic groups that are involved in the ion exchange process are fixed onto these fillers, the efficiency of the composite membranes is seen to be considerably improved. It has been noted that, in PEM fuel cells, sulphonated SiO_2 [18] and sulphonated TiO_2 [19] based composite membranes showed higher power density when compared to the commercial membrane Nafion. Chun-ChenYang et al[20] and T.S. Zhao et al [21] have proved

that the use of quaterinized silica PVA composite membrane resulted in higher hydroxyl (OH^-) conductivity as compared to non-functionalized silica based composite membrane. These results suggested that the better performance of the membranes was due to the ammonium group functionalized silica.

In the present work, mesoporous silica (SBA-15) was synthesized by template method and quaternized. It was then incorporated into quaternary polysulfone (QPSu) to form composite membrane. Mesoporous SBA-15 was chosen due to their very large surface area with uniform arrangement of hexagonal tubular channels (which are capable of holding large water molecules), with ease of surface modification. In addition, these particles also possess high mechanical and thermal stability. It was expected that upon quaternizing these mesoporous silica, the ion-exchange capacity would increase to a greater extent. The preparation, properties and performance of composite membranes incorporated with quaternized silica in fuel cell are discussed in the following sections.

2. Materials and Methods:

Polysulfone (M_w=35,000) tetraethyl ortho silicate and Pluronic P123, ($EO_{20}PO_{70}EO_{20}$) were purchased from Sigma Aldrich. Other chemicals like chloroform, methanol, triethylamine, dimethylformamide, paraformaldehyde, chlorotrimethylsilane and stannic chloride were purchased from E-Merck (India). Vulcan XC-72 (20% of Platinum in carbon support) was purchased from Arora-Mathey. Carbon cloth was obtained from Cobat carbon Inc. Double distilled water was used throughout the experiments.

2.1.1. Synthesis of Santa Barbara Amphorous (SBA-15)

The pure mesoporous SBA-15 material was prepared according to the procedure described elsewhere[22]. In general, 4.0 g of Pluronic P123, ($EO_{20}PO_{70}EO_{20}$) tri-block copolymer was added to 30 g of distilled water and stirred for 3h in order to get a clear solution, 2 M HCl (120 g) solution was gradually added into the above solution and 9 g of tetraethyl ortho silicate (TEOS) as a silica source was introduced, and the resulting mixture was allowed to stir for 20 h at 40^o C in an oil bath. The reaction mixture was transferred to teflon lined autoclave and aged at 100°C for 48h. The obtained solid product was filtered and washed with de-ionsed water and dried in an oven at 100°C for 12 hours. The resulting material obtained was then calcinated at 550°C for 12 h to remove the template.

2.1.2. Synthesis of Chloromethylated functionalized SBA-15 (CMSBA-15)

The prepared SBA-15 (1g) was well dispersed in 20 ml of dry toluene under stirring. To this solution chloropropyltriethoxysilane (3 mmol per 1g of SBA-15) was added and

refluxed under nitrogen for 24 h at 100°C [23]. After the set time, reaction mixture was filtered off to remove the solvent and excess reactants followed by washing with dichloromethane and with acetone to yield pure chloro functionalized SBA-15 (CMSBA-15) material.

2.1.3. Synthesis of quaternary ammonium SBA-15(QSBA-15)

CMSBA-15 (1g) was dispersed in 20 ml of toluene. To this triethylamine was added drop wise and the reaction was carried out under nitrogen atmosphere for 12 hours at 60ºC. Purification was similar to that mentioned for CMSBA-15.

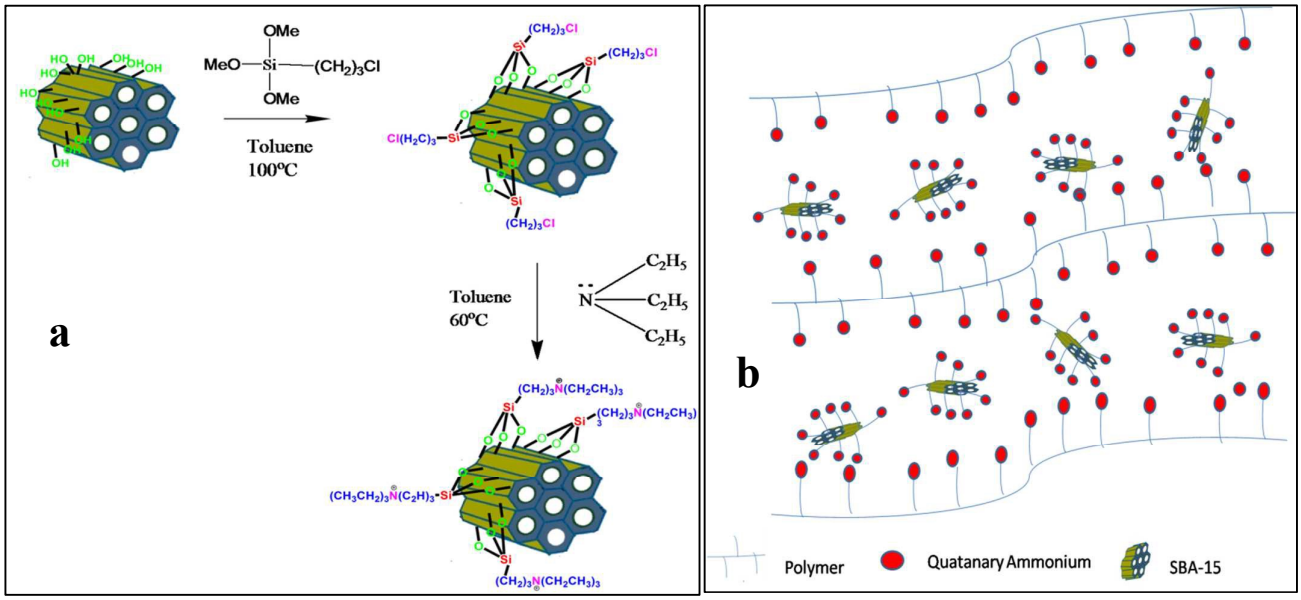

Fig.1 (a) Schematic representation of preparation of QSBA-15, (b) Composite membrane of QPSU/QSBA-15

2.1.4 Preparation of composite membrane

The preparation and characterization of quaternary ammonium functionalized polysulfone (QPSU) has been described in our previous work. [24] The QPSU in Cl^- form was dissolved in DMF and different weight proportions (1% 2%, 3% and 4%) of QSBA were added, stirred for 24 h and sonicated for 15 mins. The solutions were finally cast on a clean petridish to obtain the membranes with the desired thickness The cast membrane was dried at 70 °C for 8 h and then immersed in 1M KOH to convert Cl^- to OH^- form.

2.2. Instrumental characterization

2.2.1. FTIR

The FTIR analysis was conducted with Alpha Bruker in the spectral range from 4000 to 500 cm^{-1} to confirm the functional groups grafted on SBA-15.

2.2.2.XRD

X-ray diffraction (XRD) spectra of membrane samples were recorded using "X" Pert Pro diffractometer to study the amorphous nature. The scanning angle was 10-80° with a scanning rate of 2° per minute.

2.2.3. Morphology Study:

A scanning electron microscope (SEM) (JEM-5600LV) was used to analyze the morphology of synthesized SBA-15 mesoporous nano particle and composite membranes. For scanning electron microscopy (SEM), gold sputter coatings were carried out on the desired membrane samples at pressures ranging between 1 and 0.1 Pa. HRTEM images were produced using HRTEM Tecnai T30 to study the morphology of the functionalized SBA-15.

2.2.4. BET and Particle size analysis

Brunner Emmett Teller (BET) surface area was obtained on an Autosorb Automated Gas Sorption System (M/s. Quantachrome, USA) with N_2 as adsorbate at liquid nitrogen temperature. Total surface area and pore volumes were determined using automated surface area and pore size analyzer for the synthesized SBA-15 and QSBA-15. The mesoporosity of the samples was characterized by using a nitrogen sorption analysis.

The particle size of the SBA-15 and QSBA-15 was determined using a particle size analyzer (Zeta sizer, Malvern instruments ltd). The samples were dispersed in acetone and sonicated for 10 minutes before the experiment.

2.2.5. Mechanical Properties

The mechanical properties of the composite membranes were obtained from Hounsfield universal testing machine. The samples were cut into 5 mm width and 50 mm length and the testing was carried out in laboratory atmosphere of 25°C ± 2°C and 100% relative humidity at a cross head speed of 10 mm/min.[25] For each testing three measurements were made and the average value was reported.

2.2.6. Acceleration Stability Test

The alkaline resistance of the prepared membranes was carried out by immersing the membranes in 1mol L^{-1}aqueous KOH solution for 7 days at 60ºC, after which the loss in IEC and conductivity were measured.

2.2.7. Water Uptake and Ion-exchange capacity (IEC):

The composite membranes were dried in an oven at 80 ° C for 24 h then weighed and immersed in de-ionized water for 24 h. Then the composite membrane was taken out and the surface water was wiped away, and weighed quickly. The weight difference gives the amount of water uptake by the membrane and its was calculated by the following equation

$$\mathbf{Wut} = \frac{\mathbf{(Wwet - Wdry)}}{\mathbf{Wdry}} \times \mathbf{100\%} \qquad Eq.1$$

Where, W_{wet} is the weight of the wet composite membrane and W_{dry} is the weight of the dry membrane.

The ion exchange capacity (IEC) of the membrane was determined using back titration. The dried composite membrane in OH^- was immersed into 50 mL of standardized HCl (0.01 M) for 24 h, to convert OH^- form into Cl^- form and then a standard solution of NaOH (0.01 M) was used to titrate the HCl solution using phenolphthalein as an indicator [26]. The IEC value is given by

$$\mathbf{IEC} = \frac{\mathbf{M1V1 - M2V2}}{\mathbf{Wdry}} \qquad Eq.2$$

Where, M1 (M) and V1 (mL) are the concentration and volume of the initial HCl solution. M2 (M) and V2 (mL) are the concentrations and volumes of the standard NaOH solution used for titration. W dry (g) is the weight of the dry composite membrane.

2.2.8. Membrane conductivity

The prepared composite membrane resistance was measured by electrochemical impedance spectroscopy (EIS) using a potentiostat (BioLogic VSP, France) electrochemical system. Signal amplitude of 10 mV in the frequency range of 1 MHz to 100 Hz was applied [27]. The sample was soaked in water at 30°C for 24 h and after removing the surface water, it was sealed between two electrodes with an area of 0.62 cm^2. The impedance measurement was then carried out. The conductivity values were calculated using Eq.3

$$\sigma = L/RA \qquad Eq.3$$

Where σ is the hydroxyl conductivity of the membrane (S/cm), L is the membrane thickness (cm), R is the membrane resistance (Ω) and A is the area of the electrode (cm^2).

2.2.9. Fuel cell performance

Membrane electrode assembly (MEA) preparation was followed as per the previous work[24] with platinum anode (0.25mg/cm^{-2}) and platinum cathode (0.4mg/cm^{-2}). The prepared anode

and cathode were dried in a vacuum oven at 100 °C for 2 h and then in muffle furnace at 350 °C for 6 h. The prepared composite membranes in OH^- form were sandwiched between the prepared anode and cathode electrodes and hot pressed at 80 °C with 1.5 ton pressure for 2 minutes. The performance of the fabricated MEA was tested in an indigenous fuel cell test station. Fuel cell measurements were carried out at different temperature with H_2 and O_2 gases in the flow rate of 300 SCCM and 500 SCCM with 80% relative humidity respectively.

3. Results and discussion

3.1 Solid state NMR

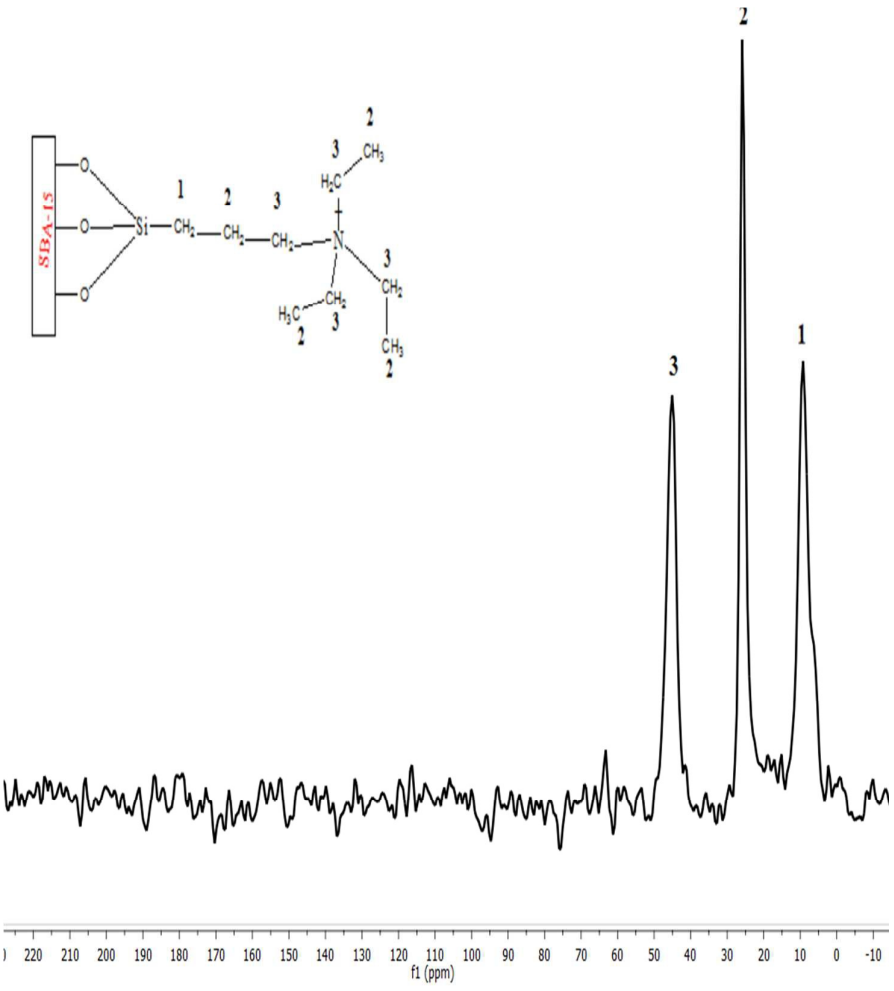

Fig. 2 Solid state ^{13}C NMR of QSBA-15

The solid state ^{13}C NMR of QSBA-15 (fig 2) shows three major peaks at 10, 25 and 46 ppm[28] corresponding to the carbons shown in the inset figure which gives additional confirmation for the presence of ammonium group grafted on the SBA-15. FTIR spectra (SF-1) of the SBA-15, CMSBA-15 and QSBA-15 are given in the supplementary section.

3.2. BET and particle size analyses

The N_2 adsorption/desorption isotherms of the QSBA-15 sample together with the pure SBA-15 sample are shown in Fig.3. The BET surface area (SBET) and total pore volume (V total) are given in Table 1. All the materials exhibited a type IV isotherm with H1 hysteresis and a sharp increase in volume adsorbed at P/P0 = 0.76, which implied that the materials possessed large pore sizes with narrow distributions. QSBA-15 also showed all the characteristics of pure SBA-15 with reduction of loop intensities due to the organic modification [29,30]. From the particle size analysis, the particle size of the QSBA-15 and SBA-15 was determined and the values are tabulated in table 2.

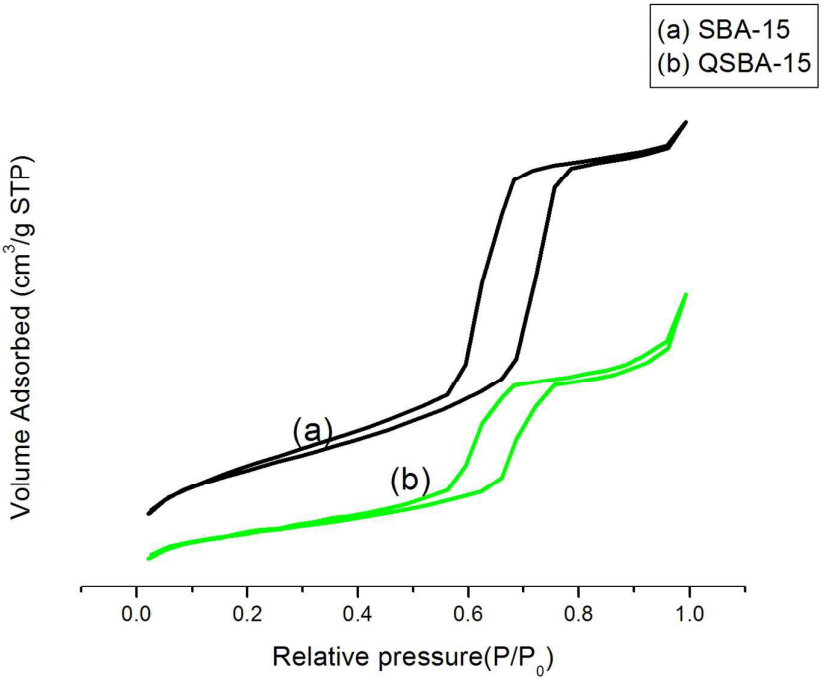

Fig. 3 N_2 adsorption/desorption isotherms of SBA-15(a) and QSBA-15(b)

Table 1 Characteristics of SBA-15 and QSBA-15

Sample	BET surface area (m^2/g)	Pore Volume (cm^3/g)	Pore size (nm)	Particle Size (nm)
SBA-15	748	1.21	9.4	786
QSBA-15	445	0.86	8.2	513

3.3. XRD:

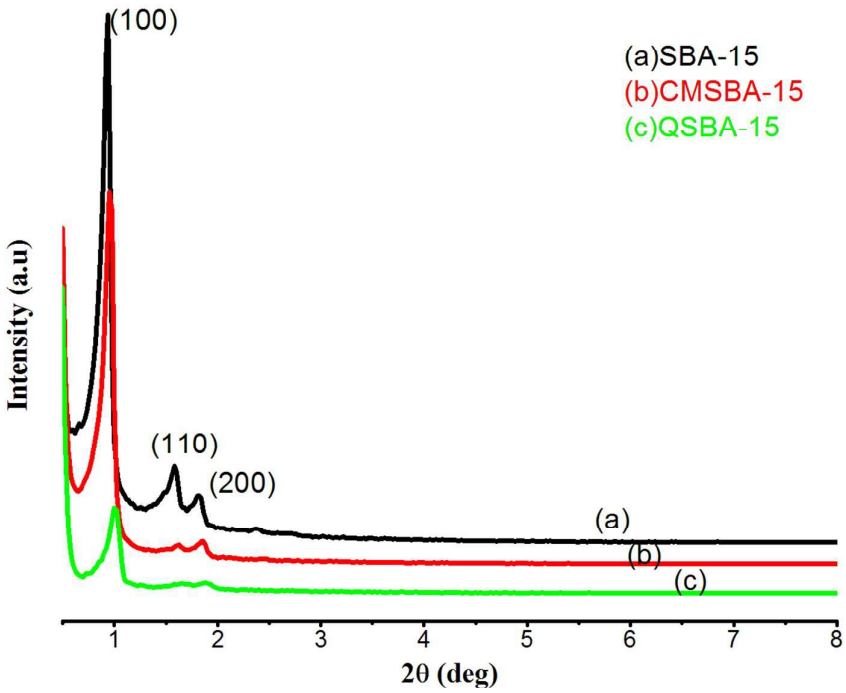

Fig. 4 Low-angle X-ray diffractions of SBA-15(a), CMSBA-15(b) and QSBA-15(c)

Fig. 4 shows the low-angle X-ray diffraction of SBA-15(a), CMSBA-15(b) and QSBA-15(c). The low angle XRD of SBA-15 materials exhibited well-resolved pattern with major peaks at $2\theta = 0.8^\circ$, 1.4° and 1.6° corresponding to (1 0 0), (1 1 0) and (2 0 0) planes,

consistent with the pattern reported for SBA-15. All the materials show the characteristic mesostructure of hexagonal space group symmetry P6mm**.** When compared to spectrum a (SBA-15), the intensities of all the peaks in spectrum b (CMSBA-15) decreased. Further, it decreased in spectrum c (QSBA-15) indicating the surface functionalization. This also suggested that the structural order was reduced maintaining the basic structure of SBA-15 [28] which was reflected in the results of the TEM.

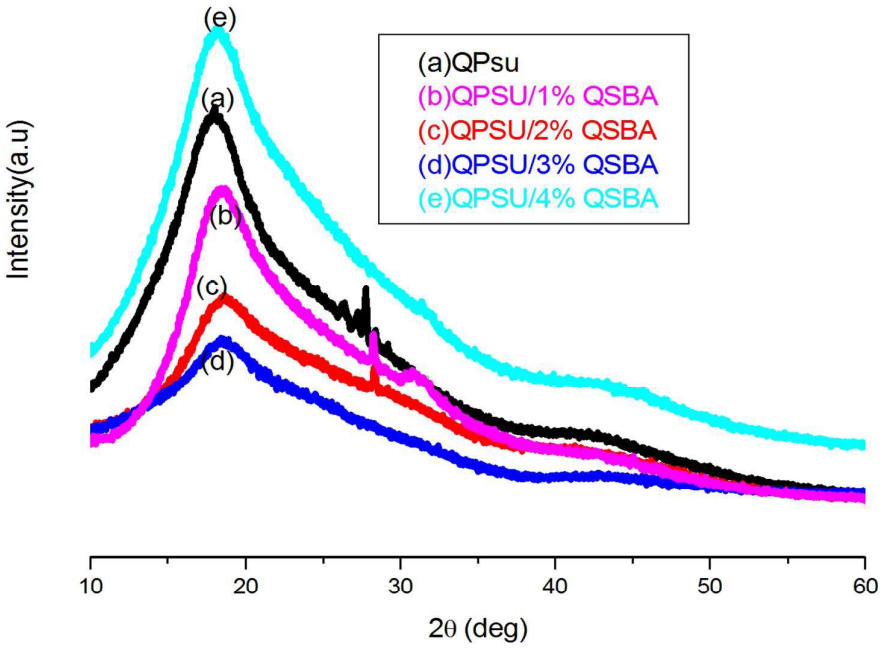

Fig. 5 XRD spectra of QPSU(a) QPSU/1% QSBA(b) QPSU/2% QSBA(c) QPSU/3% QSBA(d) and QPSU/4% QSBA(e)

Fig.5 shows the XRD patterns of QPSU and various QPSU-QSBA composite membranes. From the XRD profiles, it can be seen that peak intensity at 2θ = 19-20° (which are due to the polymer backbone) decreased with increase in the concentration of QSBA from 1% to 3 % thus increasing the amorphous nature of the composite membranes. Ionic conductivity of the membranes is closely associated with the crystallinity of materials. Low crystallinity increased the transport of ions in the membrane[31]. 3% of filler loading highly decreased the crystallinity and showed the highest ionic conductivity. Further increase in the addition of QSBA fillers to 4% resulted in increased crystalline properties.

3.4. Morphology studies

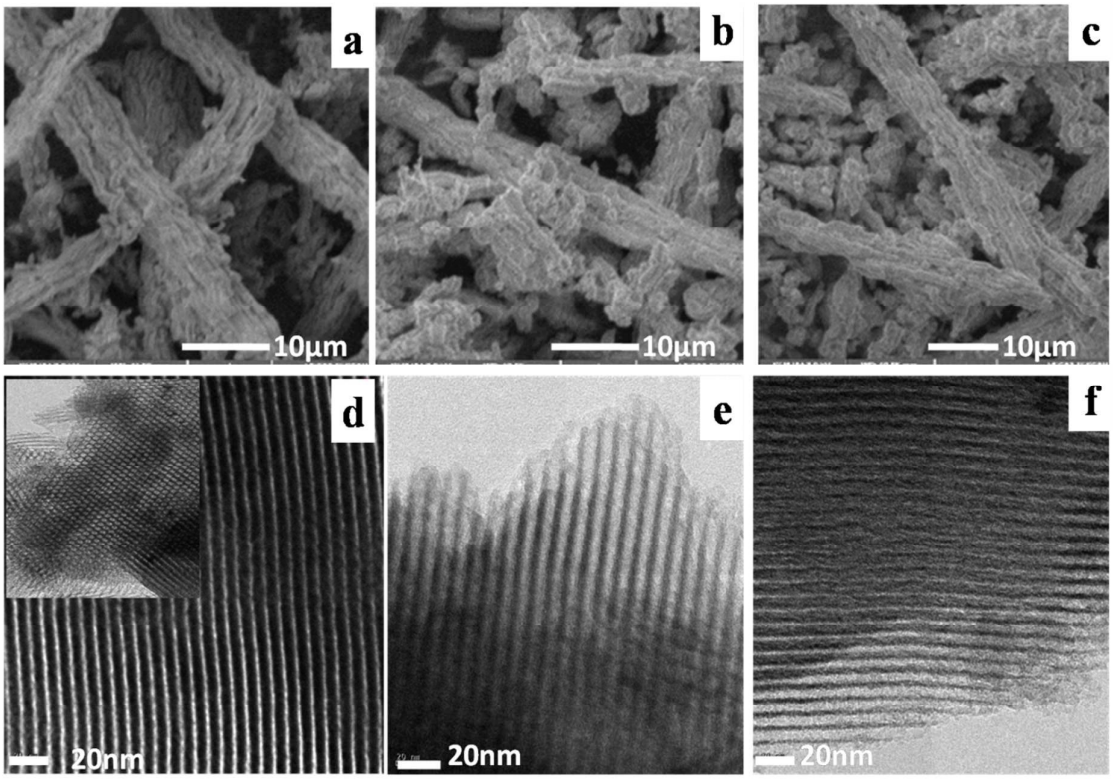

Fig. 6 SEM images of SBA-15(a),CMSBA-15(b),QSBA-15(c) and TEM images SBA-15(d),CMSBA-15(e),QSBA-15(f) taken perpendicular to the pore axis; Inset (d) SBA-15 along the pore axis.

3.5. Membrane Characterization

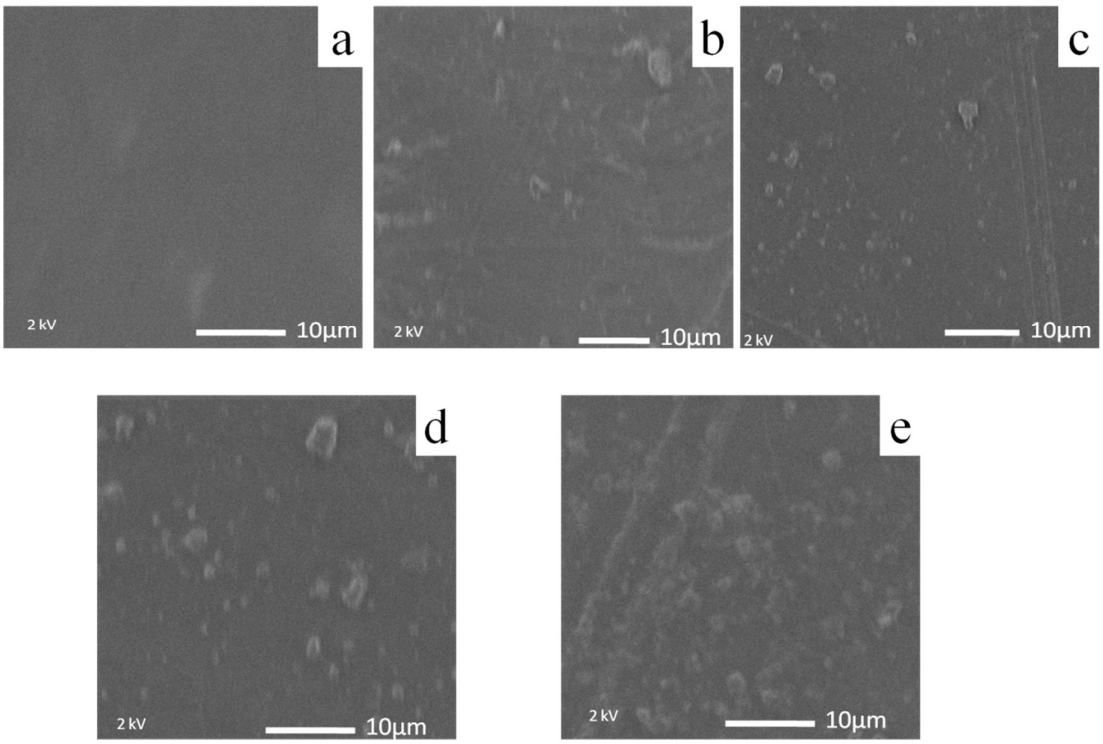

Fig. 7 SEM images of QPSU (a) QPSU/1% QSBA(b) QPSU/2% QSBA(c) QPSU/3% QSBA(d) and QPSU/4% QSBA(e).

The SEM images, shown in fig 6a, b and c clearly depicted the uniform distribution of the cylindrical shape of SBA -15. Figure 6d of HR-TEM analyses showed a well ordered 2D hexagonal arrays present in the mesoporous structure of SBA-15 while fig 6 e & f suggested that the structure of SBA-15 was retained even after chloromethylation and subsequent grafting with ammonium groups[32]. Fig 7(a) showed the homogeneous and smooth surface of QPSU membrane and the images of figures 7 b-d confirmed the presence of QSBA-15 filler particles and their homogeneous distribution throughout the surface of the composite membranes. This homogenous distribution of the fillers occurred mainly because of the hydrophilic nature of both QPSU polymer as well as QSBA fillers. In addition, it was also inferred from fig. 7 b-d that membranes up to 3 % of filler loading were not associated with any phase separation since the filler QSBA was observed to be uniformly impregnated into the polymer matrix. However, in case of higher filler loading above 3% (fig 7e), the membrane's morphology becomes slightly non-homogeneous due to particle agglomeration. This observation was also seen in the XRD spectra, where beyond 3% filler, the crystallinity of the composite membrane increased.

3.6. Mechanical property

The results of the tensile strength of QPSU and their corresponding composite membranes are shown in Fig. 8. From the figure, it was noted that the tensile strength of QPSU/QSBA composite membranes was higher than QPSu membrane which was due to the addition of the SBA-15 fillers which played two roles: one to act as a reinforcement and second, the fillers increased the water uptake and thus contributing to an increase in the elastic property of the composites. It should also be emphasized that however, an excessive increase in concentration beyond an optimum level may possibly lead to aggregation of the filler particles and eventually causes catastrophic failure.[33] This effect is reflected in the inferior tensile strength of the composite with 4 wt% QSBA-15 as compared with 3 wt% QSBA-15 filler composites.

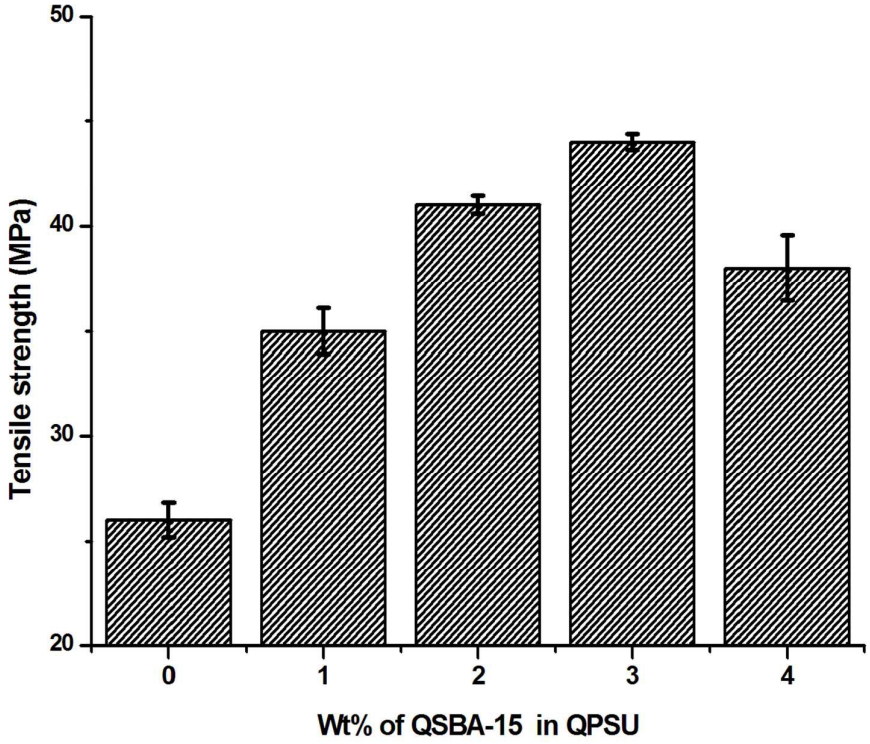

Fig .8 Mechanical property of composite membrane

3.7. Water uptake, Ion Exchange Capacity and Conductivity studies

Ion-exchange capacity, which is one of the fundamental characteristics of ion-exchange membranes, was found to increase with the addition of QSBA-15 fillers to the QPSU membrane as shown in table 2. This high ion exchange property was attributed to the presence of additional ammonium groups in the functionalized SBA-15 in addition to the ammonium groups present in the polymer matrix. Further, from table 2, it was also noted that the water uptake capacity of the composite membranes increased with the addition of QSBA-15. This higher water uptake of the composite membranes over the QPSU membrane was due to the porous cylindrical nature of the QSBA-15 fillers that possess the capacity to hold more water. It was further noted that, both IEC and water uptake capacity of the membranes increased with the increase in QSBA-15 concentration and this trend was observed in the range of 1-3 wt%. of QSBA-15. However, on higher QSBA-15 loading, it was observed that in contrary to our expectation, there was a slight dip in the values of IEC and water uptake from that of 3% QSBA-15. This decrease was explained by considering that the addition of 4% QSBA-15 resulted in agglomeration of the fillers within the QPSu matrix as evidenced in the SEM image (fig. 8e) along with an increase in the crystallinity as shown in the XRD

image (Fig.6e). A similar trend was also observed in the case of membrane conductivity before and after acceleration tests. The decrease in conductivity after accelerated test is due to the hydrolysis of ether linkage and ylide formation of QPSu[34] . It was found that the loss in IEC and conductivity of the membranes after the degradation were of acceptable level and maintained almost in the same order. From the above results, it was clear that the composite membrane having 3% QSBA-15 showed the most favourable property amongst all the fabricated membranes. It also needs to be noted that the values observed for QPSu with quarternary ammonium functionalized SBA-15 was much better than our previously reported values for QPSu membranes with un-fuctionalized fillers and the values reported herein were comparable to those reported in literature (Table 3). This further provides evidence to the observation that the use of functionalized fillers would show enhanced efficiency in the membrane as compared with un-functionalized fillers. The water absorption, IEC and conductivity values of the commercial membrane (AMI-7001) have also been included in the table for comparison.

Table 2: Properties of the membranes

Membrane	Membrane thickness (μm)	Water absorption (%)	Before Accelerated Stability Test		After Accelerated Stability Test	
			IEC (meq/g)	Conductivity (S/cm)	IEC (meq/g)	Conductivity (S/cm)
AMI-7001*		17	1.3	1.72×10^{-2}	-	-
QPSU	95±5	5.43	0.681	0.68×10^{-2}	0.624	0.57×10^{-2}
QPSU/1% QSBA	98±3	12.56	1.295	1.19×10^{-2}	1.194	1.04×10^{-2}
QPSU/2% QSBA	100±5	14.72	1.562	1.48×10^{-2}	1.436	1.29×10^{-2}
QPSU/3% QSBA	96±4	17.32	1.743	1.80×10^{-2}	1.654	1.59×10^{-2}
QPSU/4% QSBA	99±6	15.62	1.612	1.61×10^{-2}	1.475	1.39×10^{-2}

*AMI-7001 – Divinylbenzene crosslinked polystyrene functionalized with quaternary ammonium groups.

3.8. Fuel Cell Evaluation:

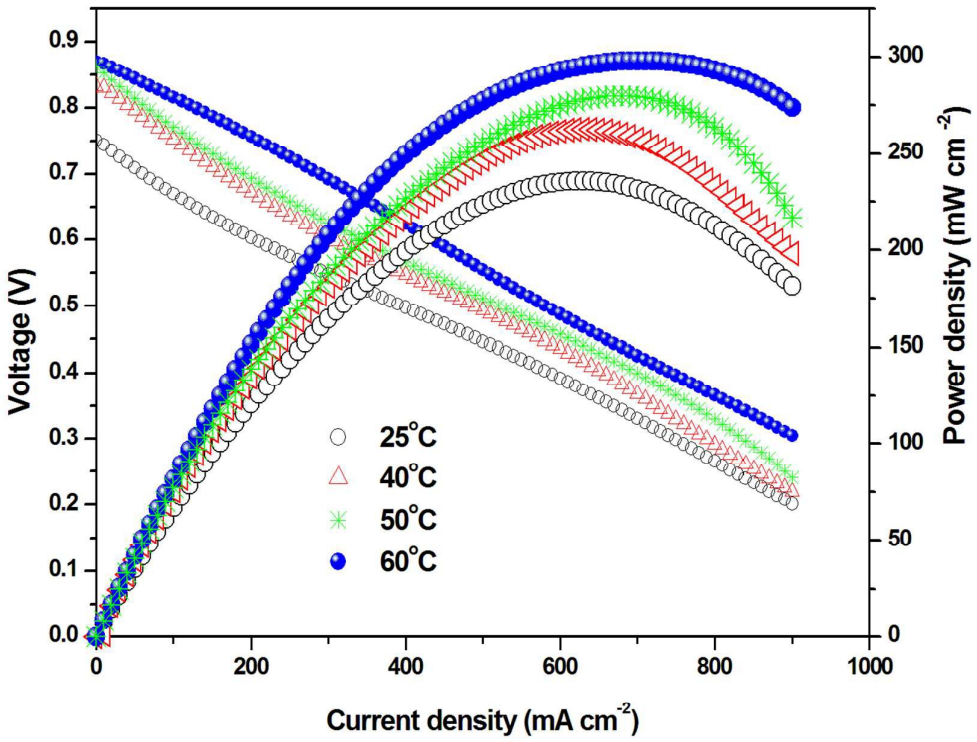

Fig. 9 Polarization curves of 3% QSBA/QPSU membrane different temperature

Fig. 9 shows the polarization curves of the fabricated 3% QSBA/QPSU membrane as tested in a single cell (25 cm^2) AFC at different operating temperatures using Pt as catalyst for both anode and cathode electrodes. The performance of the single cell AFC was maximum at 60ºC due to higher hydroxyl conductivity, water retention properties of the composite membranes and better electrode kinetics. The composite membrane showed the maximum OCV of 0.86 V and a maximum power density of 298 mW/cm^2 at 60ºC. These power density values were higher and comparable with those of previously reported values of QPSU/SiO_2, QPSU/ZrO_2 and other similar composite membranes which are given in table 3.

Table 3 Comparison of various composite AEM published in literature.

Membrane	IEC, meq/g	Conductivity, S/cm	Power density mW/cm^2	Reference
QPSU/QSBA-15	1.743	1.80 x 10^{-2}	298	present work
QPSU/MWCNT	0.792	0.84 x 10^{-2}	190	[35]
QPSU/SiO_2	1.37	1.63 x 10^{-2}	252	[36]
QPSU/ZrO_2	0.921	1.51 x 10^{-2}	214.5	[24]
PAES/ ZrO_2	1.82	0.23 x 10^{-2}	----	[37]
PE-TEA	1.097	0.29 x 10^{-2}	90	[38]
QAPS/PTFE	1.27	0.31 x 10^{-2}	315	[7]
PABMHM	1.416	0.24 x 10^{-2}	…..	[39]

[PAES-Poly (arylene ether sulfone), PE-TEA - Porous Polyethylene-Triethylamine, QAPS-Quaternary ammonia polysulfone and PABMHM - Poly(1-allyl-3-(6-(1-butyl-2-methylimidazol-3-ium-3-yl)hexyl)-2-methylimidazole].

4. Conclusion:

High surface area (754 m^2/g) mesoporous SBA-15 was synthesized and quateranary ammonium was successfully grafted without affecting the texture of SBA-15. This was confirmed using NMR, FT-IR, XRD, BET, SEM and TEM techniques. Composite membranes were fabricated using the QSBA-15 dispersed in QPSu polymer matrix and various studies were carried out to determine its suitability for alkaline fuel cell application. From the study, it was inferred that the composite membrane with 3 wt% QSBA-15 loading displayed the optimum properties of ion exchange capacity, water uptake and conductivity for fuel cell application. The performance of the QPSU/3% QSBA membrane was evaluated in the alkaline fuel cell set up where an OCV of 0.86 V and a power density of 298 mW/cm^2 were achieved at an operating temperature of 60ºC. The results suggest that the functionalized nano fillers would serve to overcome the issues related to the physico-chemical stability of polymer electrolyte membranes with high degree of functionalization for high performance in fuel cells.

Acknowledgement:

The authors thank Council of Scientific and industrial research (CSIR), New Delhi, India for their financial support (Vide letter No. 01(2452)/11/EMR-11, letter dated 16.05.2011).

Reference

1. Y. Ye, S. Sharick, E. M. Davis, K. I. Winey and Y. a. Elabd, *ACS Macro Lett.*, 2013, **2**, 575–580.

2. W. Lu, Z.-G. Shao, G. Zhang, Y. Zhao, J. Li and B. Yi, *Int. J. Hydrogen Energy*, 2013, **38**, 9285–9296.

3. H. Zarrin, J. Wu, M. Fowler and Z. Chen, *J. Memb. Sci.*, 2012, **394-395**, 193–201.

4. Y. Zha, M. L. Disabb-Miller, Z. D. Johnson, M. a Hickner and G. N. Tew, *J. Am. Chem. Soc.*, 2012, **134**, 4493–6.

5. X. Lin, Y. Liu, S. D. Poynton, A. L. Ong, J. R. Varcoe, L. Wu, Y. Li, X. Liang, Q. Li and T. Xu, *J. Power Sources*, 2013, **233**, 259–268.

6. C. G. Arges, V. Ramani and P. N. Pintauro, *Elctrochemical Soc. Interface*, 2010, 31–35.

7. Y. Zhao, J. Pan, H. Yu, D. Yang, J. Li, L. Zhuang, Z. Shao and B. Yi, *Int. J. Hydrogen Energy*, 2013, **38**, 1983–1987.

8. B. P. Tripathi, M. Kumar and V. K. Shahi, *J. Memb. Sci.*, 2010, **360**, 90–101.

9. M. R. Hibbs, C. H. Fujimoto and C. J. Cornelius, *Macromolecules*, 2009, **42**, 8316–8321.

10. C. Klaysom, S.-H. Moon, B. P. Ladewig, G. Q. M. Lu and L. Wang, *J. Memb. Sci.*, 2011, **371**, 37–44.

11. J. John, K. M. Hugar, J. Rivera-Meléndez, H. A. Kostalik, E. D. Rus, H. Wang, G. W. Coates and H. D. Abruña, *J. Am. Chem. Soc.*, 2014.

12. N. Li, Y. Leng, M. a Hickner and C.-Y. Wang, *J. Am. Chem. Soc.*, 2013, **135**, 10124–33.

13. K. Matsumoto, T. Fujigaya, H. Yanagi and N. Nakashima, *Adv. Funct. Mater.*, 2011, **21**, 1089–1094.

14. J. Pan, Y. Li, J. Han, G. Li, L. Tan, C. Chen, J. Lu and L. Zhuang, *Energy Environ. Sci.*, 2013, **6**, 2912.

15. P. K. Leung, Q. Xu, T. S. Zhao, L. Zeng and C. Zhang, *Electrochim. Acta*, 2013, **105**, 584–592.

16. P. T. Nonjola, M. K. Mathe and R. M. Modibedi, *Int. J. Hydrogen Energy*, 2013, **38**, 5115–5121.

17. C. Klaysom, S.-H. Moon, B. P. Ladewig, G. Q. M. Lu and L. Wang, *J. Colloid Interface Sci.*, 2011, **363**, 431–9.

18. J.-H. Won, H.-J. Lee, K.-S. Yoon, Y. T. Hong and S.-Y. Lee, *Int. J. Hydrogen Energy*, 2012, **37**, 9202–9211.

19. C. H. Rhee, Y. Kim, J. S. Lee, H. K. Kim and H. Chang, *J. Power Sources*, 2006, **159**, 1015–1024.

20. C.-C. Yang, S.-S. Chiu, S.-C. Kuo and T.-H. Liou, *J. Power Sources*, 2012, **199**, 37–45.

21. E. D. Wang, T. S. Zhao and W. W. Yang, *Int. J. Hydrogen Energy*, 2010, **35**, 2183–2189.

22. H.-M. Kao, C.-C. Ting and S.-W. Chao, *J. Mol. Catal. A Chem.*, 2005, **235**, 200–208.

23. R. Srivastava, *J. Mol. Catal. A Chem.*, 2007, **264**, 146–152.

24. R. Vinodh, M. Purushothaman and D. Sangeetha, *Int. J. Hydrogen Energy*, 2011, **36**, 7291–7302.

25. F. Mammeri, L. Bourhis and C. Sanchez, 2005, 3787–3811.

26. L.-Y. Yu, Z.-L. Xu, H.-M. Shen and H. Yang, *J. Memb. Sci.*, 2009, **337**, 257–265.

27. S. Ayyaru and S. Dharmalingam, *RSC Adv.*, 2013, **3**, 25243.

28. S.-Y. Chen, C.-Y. Huang, T. Yokoi, C.-Y. Tang, S.-J. Huang, J.-J. Lee, J. C. C. Chan, T. Tatsumi and S. Cheng, *J. Mater. Chem.*, 2012, **22**, 2233.

29. N. Fattori, C. M. Maroneze, L. P. Costa, M. Strauss, F. A. Sigoli, I. O. Mazali and Y. Gushikem, 2012.

30. K. Northcott, H. Kokusen, Y. Komatsu and G. Stevens, *Sep. Sci. Technol.*, 2006, **41**, 1829–1840.

31. Y. Xiong, Q. L. Liu and Q. H. Zeng, *J. Power Sources*, 2009, **193**, 541–546.

32. X. Wang, P. Wang, Z. Dong, Z. Dong, Z. Ma, J. Jiang, R. Li and J. Ma, *Nanoscale Res. Lett.*, 2010, **5**, 1468–1473.

33. Y. Wu, C. Wu, J. R. Varcoe, S. D. Poynton, T. Xu and Y. Fu, *J. Power Sources*, 2010, **195**, 3069–3076.

34. C. G. Arges and V. Ramani, *Proc. Natl. Acad. Sci. U. S. A.*, 2013, **110**, 2490–2495.

35. R. Vinodh and D. Sangeetha, , **4**.

36. R. Vinodh and D. Sangeetha, *Int. J. Green Energy*, 2012, 121210071952007.

37. X. Li, Y. Yu and Y. Meng, ACS Appl. Mater. Interfaces 2013, **5**, 1414−1422.

38. S. Maurya, S. H. Shin, M. K. Kim, S. H. Yun and S. H. Moon, *J. Memb. Sci.*, 2013, **443**, 28–35.

39. B. Qiu, B. Lin, Z. Si, L. Qiu, F. Chu, J. Zhao and F. Yan, *J. Power Sources*, 2012, **217**, 329–335.